2-1-1984

Laminar Condensation on a Moving Drop. Part 2. Numerical Solutions

J. N. Chung
Washington State University

Portonovo S. Ayyaswamy
University of Pennsylvania, ayya@seas.upenn.edu

Satwindar S. Sadhal
University of Southern California

Laminar Condensation on a Moving Drop. Part 2. Numerical Solutions

Abstract
In this paper, we investigate the problem of transient laminar condensation on a moving drop by the semianalytical series-truncation method. The objectives are to assess the validity and the accuracy of the matched-asymptotic method employed in Part 1 . The fluid flow and thermodynamic variables are expanded as complete series of Legendre polynomials. The resulting transient momentum, energy and species equations are integrated numerically. The numerical scheme basically involves a three-point central difference for the spatial derivatives and a backward difference expression for the temporal derivatives. The finite-difference equations have been solved by the strongly implicit procedure. Good agreement of the fully transient numerical results with the singular perturbation approximation results of Part 1 lends credibility to a quasi-steady treatment of the continuous phase. The computational time requirements for the fully numerical solutions increase with decreasing non-condensable gas mass fraction in the bulk environment.

Disciplines
Engineering | Mechanical Engineering

Comments
Suggested Citation:
Chung, J.N. and Portonovo S. Ayyaswamy. (1984) *Laminar condensation on a moving drop. Part 2. Numerical solutions.* Journal of Fluid Mechanics. Vol. 139, p. 131-144.

J. Fluid Mech. (1984), *vol.* 139, *pp.* 131–144
Printed in Great Britain

Laminar condensation on a moving drop. Part 2. Numerical solutions

By J. N. CHUNG,
Department of Mechanical Engineering, Washington State University, Pullman, WA 99164–2920

P. S. AYYASWAMY
Department of Mechanical Engineering and Applied Mechanics, University of Pennsylvania, Philadelphia, PA 19104

AND S. S. SADHAL
Department of Mechanical Engineering, University of Southern California, Los Angeles, CA 90089–1453

(Received 26 August 1981 and in revised form 7 September 1983)

In this paper, we investigate the problem of transient laminar condensation on a moving drop by the semianalytical series-truncation method. The objectives are to assess the validity and the accuracy of the matched-asymptotic method employed in Part 1. The fluid flow and thermodynamic variables are expanded as complete series of Legendre polynomials. The resulting transient momentum, energy and species equations are integrated numerically. The numerical scheme basically involves a three-point central difference for the spatial derivatives and a backward difference expression for the temporal derivatives. The finite-difference equations have been solved by the strongly implicit procedure. Good agreement of the fully transient numerical results with the singular perturbation approximation results of Part 1 lends credibility to a quasi-steady treatment of the continuous phase. The computational time requirements for the fully numerical solutions increase with decreasing non-condensable gas mass fraction in the bulk environment.

1. Introduction

In this paper both the phases are treated as fully transient. The entire set of transient coupled equations are simultaneously solved by the series-truncation method. The flow field, fluid temperature and the mass fraction of the non-condensable gas are expanded as complete series of Legendre polynomials. The basis of the series-truncation method is to approximate the solutions by a finite number of terms (Van Dyke 1965; Dennis, Walker & Hudson 1973). Here a six-term expansion series has been employed. In addition to a fully transient treatment, the present analysis provides results of a higher accuracy, particularly for high rates of condensation, compared with those presented in Part 1 (Chung, Ayyaswamy & Sadhal 1984). In Part 1 the expansion series was truncated after $P_1(\cos\theta)$ in view of the analytical treatment being very difficult and involved. As a consequence, some of the results for the high-condensation regime (strong flow field, high liquid-side Péclet number Pe_ℓ and $Re_c \sim 5$) provided there may not be sufficiently accurate. In the present paper the series has been truncated only after $P_6(\cos\theta)$. Larger values for Pe_ℓ have been

accommodated and we are able to provide accurate results for high condensation rates. Finally, by comparing the numerical results obtained here with the results of Part 1, we have ascertained the validity of the quasi-steady assumption for the continuous phase.

2. Theoretical formulation

We now drop the assumption that the fluid motion, and the heat and mass transfer in the continuous phase could be treated as quasi-steady. The other assumptions are identical with those made in Part 1. Non-dimensionalization will be as in Part 1 unless otherwise indicated.

2.1. *Continuous phase* ($r > 1$)

We set the velocity components

$$u_r = -\frac{1}{r^2}\frac{\partial \psi}{\partial \bar{\mu}}, \quad u_\theta = -\frac{1}{r\sin\theta}\frac{\partial \psi}{\partial r}, \tag{1}$$

where ψ is the stream function and $\bar{\mu} = \cos\theta$.

The dimensionless time-dependent momentum equation in terms of the stream function ψ is

$$\frac{\partial \mathrm{D}_r^2 \psi}{\partial t} + Re_\infty \left\{\frac{1}{r^2}\frac{\partial(\psi, \mathrm{D}_r^2\psi)}{\partial(r,\bar{\mu})} + \frac{2}{r^2}(\mathrm{D}_r^2\psi)\,\mathrm{L}_r\psi\right\} = \mathrm{D}_r^4\psi, \tag{2}$$

where

$$\boldsymbol{u} = \boldsymbol{\nabla}\times\left(\frac{\psi(r,\theta)}{r\sin\theta}\right)\boldsymbol{i}_\phi. \tag{3}$$

$\boldsymbol{i}_\phi$ is the unit vector in the azimuthal direction. The time t has been scaled by R^2/ν_∞. In (2)

$$\mathrm{D}_r^2 = \frac{\partial^2}{\partial r^2} + \frac{1-\bar{\mu}^2}{r^2}\frac{\partial^2}{\partial \bar{\mu}^2}, \tag{4}$$

$$\mathrm{L}_r = \frac{\bar{\mu}}{1-\bar{\mu}^2}\frac{\partial}{\partial r} + \frac{1}{r}\frac{\partial}{\partial \bar{\mu}}. \tag{5}$$

Consider the translation of the droplet as a perturbation of the condensation-induced radial field. Then we can write

$$\psi = [-A_{00}(t)\,Q_0(\bar{\mu})] + \epsilon\psi_1, \quad \psi_1 = O(1), \tag{6}$$

where

$$Q_m(\bar{\mu}) = \int_{-1}^{\bar{\mu}} P_m(\mu')\,\mathrm{d}\mu', \tag{7}$$

in which $P_m(\bar{\mu})$ is the Legendre polynomial of order m. In (6) $\epsilon = Re_\infty(t) = U_\infty(t)\,R/\nu_\infty$, $A_{00} = A_0\,R/\nu_\infty$, and A_0 is the normal velocity as in Part 1. Here ψ and ψ_1 have been scaled with $\nu_\infty R$ and $U_\infty R^2$ respectively, as was done in Sadhal & Ayyaswamy (1983). Upon substituting (6) into (2) and collecting terms of $O(\epsilon)$, we have

$$\frac{\partial \mathrm{D}_r^2\psi_1}{\partial t} + \frac{A_{00}}{r^2}\frac{\partial \mathrm{D}_r^2\psi_1}{\partial r} - 2\frac{A_{00}}{r^3}\mathrm{D}_r^2\psi_1 = \mathrm{D}_r^4\psi_1. \tag{8}$$

We now cast (8) in terms of the vorticity ζ, and transform the radial coordinate as

$r = e^{\xi}$, to facilitate numerical computation. In terms of the new variable ξ the vorticity equation may be written as

$$\frac{\partial^2 \psi_1}{\partial \xi^2} - \frac{\partial \psi_1}{\partial \xi} + \sin^2\theta \frac{\partial^2 \psi_1}{\partial \bar{\mu}^2} + \zeta e^{3\xi} \sin\theta = 0, \tag{9}$$

and (8) becomes

$$\frac{\partial \zeta}{\partial t} + e^{-3\xi} A_{00}\left(\frac{\partial \zeta}{\partial \xi} - \zeta\right) = \left(\frac{\partial^2 \zeta}{\partial \xi^2} + \frac{\partial \zeta}{\partial \xi} + \sin^2\theta \frac{\partial^2 \zeta}{\partial \bar{\mu}^2} - 2\cos\theta \frac{\partial \zeta}{\partial \bar{\mu}} - \frac{\zeta}{\sin^2\theta}\right) e^{-2\xi}. \tag{10}$$

Equations (9) and (10) are simultaneously solved subject to appropriate initial and boundary conditions. These conditions will be discussed after the mathematical model of the internal flow is presented.

2.2. *Condensed phase* ($0 \leqslant r \leqslant 1$)

The liquid-phase Reynolds number Re_ℓ will be small enough (even with Re_c as much as five) so that the inertial terms in the momentum equation for the liquid side may be neglected. The governing equation for flow is

$$\frac{\partial D_r^2 \psi_\ell}{\partial t} = D_r^4 \psi_\ell, \tag{11}$$

where time t has been scaled by R^2/ν_ℓ and ψ_ℓ has been scaled by $U_\infty R^2$. In a manner similar to the treatment of the continuous phase, we develop the stream-function–vorticity combinations for the flow calculation as

$$D_r^2 \psi_\ell + \zeta_\ell r \sin\theta = 0, \tag{12}$$

$$\frac{\partial \zeta_\ell}{\partial t} = \frac{\partial^2 \zeta_\ell}{\partial r^2} + \frac{2}{r}\frac{\partial \zeta_\ell}{\partial r} + \frac{\sin\theta}{r^2}\left[\sin\theta \frac{\partial^2 \zeta_\ell}{\partial \bar{\mu}^2} - 2\cot\theta \frac{\partial \zeta_\ell}{\partial \bar{\mu}} - \frac{\zeta_\ell}{\sin^3\theta}\right]. \tag{13}$$

2.3. *Boundary conditions, initial conditions and interface conditions*

Continuous phase

$$\psi_1 \to \tfrac{1}{2} e^{2\xi} \sin^2\theta, \quad \zeta \to 0 \quad \text{as} \quad \xi \to \infty, \tag{14}$$

$$\psi_1 = -\left(r^2 + \frac{1}{2r(1+\phi_\mu)} - \frac{3+2\phi_\mu}{2(1+\phi_\mu)} r\right) Q_1(\bar{\mu}) \quad (t = 0), \tag{15}$$

where $\phi_\mu = \mu_\infty/\mu_\ell$.

For the condensed phase

$$\psi_\ell \to 0, \quad \zeta_\ell \to 0 \quad \text{as} \quad r \to 0, \tag{16}$$

$$\psi_\ell = -(r^4 - r^2) Q_1(\bar{\mu}) \quad (t = 0). \tag{17}$$

The interface conditions, at $r = 1$, are

(i) continuity of tangential velocities and no mass transfer in the liquid phase:

$$\frac{\partial \psi_1}{\partial \xi} = \frac{\partial \psi_\ell}{\partial r}, \quad \frac{\partial \psi_\ell}{\partial \bar{\mu}} = 0; \tag{18}$$

(ii) continuity of shear stress:

$$\phi_\mu\left(\frac{\partial^2 \psi_1}{\partial \xi^2} - 2\frac{\partial \psi_1}{\partial \xi} - \sin^2\theta \frac{\partial^2 \psi_1}{\partial \bar{\mu}^2}\right) = \frac{\partial^2 \psi_\ell}{\partial r^2} - 2\frac{\partial \psi_\ell}{\partial r} - \sin^2\theta \frac{\partial^2 \psi_\ell}{\partial \bar{\mu}^2}. \tag{19}$$

2.4. *Flow equations for the series-truncation procedure*

Following the procedure for the series-truncation method proposed by Van Dyke (1965), we express ψ and ζ in terms of the Legendre and the first associated Legendre functions of order n. Thus

$$\psi_1 = e^{\frac{1}{2}\xi} \sum_{n=1}^{\infty} f_n(t,\xi) \int_{-1}^{\bar{\mu}} P_n(z)\,dz, \tag{20}$$

$$\psi_\ell = \sum_{n=1}^{\infty} F_n(t,r) \int_{-1}^{\bar{\mu}} P_n(z)\,dz, \tag{21}$$

$$\zeta = \sum_{n=1}^{\infty} g_n(t,\xi)\, P_n^{(1)}(\bar{\mu}), \tag{22}$$

$$\zeta_\ell = \sum_{n=1}^{\infty} G_n(t,r)\, P_n^{(1)}(\bar{\mu}). \tag{23}$$

With (20)–(23), the vorticity and momentum equations (9), (10), (12) and (13) become

$$f_n'' - (n+\tfrac{1}{2})^2 f_n - n(n+1)\, e^{\frac{1}{2}\xi} g_n = 0, \tag{24}$$

$$\frac{\partial g_n}{\partial t} + e^{-3\xi} A_{00}(g_n' - g_n) = (g_n'' + g_n' - n(n+1)\, g_n)\, e^{-2\xi}, \tag{25}$$

$$F_n'' - \frac{n(n+1)}{r^2} F_n - n(n+1)\, r G_n = 0, \tag{26}$$

$$\frac{\partial G_n}{\partial t} = G_n'' + \frac{2G_n'}{r} - \frac{n(n+1)}{r^2} G_n. \tag{27}$$

The transformed boundary conditions, initial conditions and interface conditions are as follows.

For the continuous phase

$$f_n = -e^{\frac{3}{2}\xi}\delta_{n1} \quad \text{as} \quad \xi \to \infty, \quad \delta_{n1} = \begin{cases} 1 & (n=1), \\ 0 & (n \neq 1), \end{cases} \tag{28}$$

$$g_n \to 0 \quad \text{for all } n, \quad \text{as} \quad \xi \to \infty, \tag{29}$$

$$\left.\begin{aligned} f_1(0,\xi) &= -\left(e^{\frac{3}{2}\xi} + \frac{e^{-\frac{3}{2}\xi}}{2(1+\phi_\mu)} - \frac{3+2\phi_\mu}{2(1+\phi_\mu)} e^{\frac{1}{2}\xi}\right), \\ f_n(0,\xi) &= 0 \quad (n \neq 1) \end{aligned}\right\} \quad (t=0). \tag{30}$$

For the condensed phase

$$F_n \to 0 \quad \text{as} \quad r \to 0, \tag{31}$$

$$G_n \to 0 \quad \text{as} \quad r \to 0, \tag{32}$$

$$F_1(0,r) = -(r^4 - r^2), \quad F_n(0,r) = 0 \quad (n \neq 1;\ t=0). \tag{33}$$

The interface conditions, at $r = 1$, are the following: (18) and (19) become

$$F_n' = \tfrac{1}{2} f_n + f_n', \quad F_n = 0, \tag{34}$$

$$F_n'' - 2F_n' + n(n+1)\, F_n = \phi_\mu [f_n'' - 2f_n' + \tfrac{1}{4}(4n^2 + 4n - 5) f_n]; \tag{35}$$

(24)–(27) are subject to conditions (28)–(35).

3. Heat and mass transfer

For a fully numerical treatment, a single approach applicable to both the low- and the high-condensation regimes is suitable.

3.1. *Vapour–gas phase*

The dimensionless energy and species equations are (omitting asterisks)

$$\frac{\partial^2 T}{\partial \xi^2}+\frac{\partial T}{\partial \xi}+\frac{\partial}{\partial \bar{\mu}}(1-\bar{\mu}^2)\frac{\partial T}{\partial \bar{\mu}} = Pr\,e^{\xi}\left(u_r\frac{\partial T}{\partial \xi}-u_\theta \sin\theta\frac{\partial T}{\partial \bar{\mu}}\right)+\frac{\partial T}{\partial t}e^{2\xi}, \tag{36}$$

$$\frac{\partial^2 w}{\partial \xi^2}+\frac{\partial w}{\partial \xi}+\frac{\partial}{\partial \bar{\mu}}(1-\bar{\mu}^2)\frac{\partial w}{\partial \bar{\mu}} = Sc\,e^{\xi}\left(u_r\frac{\partial w}{\partial \xi}-u_\theta \sin\theta\frac{\partial w}{\partial \bar{\mu}}\right)+\frac{\partial w}{\partial t}e^{2\xi}, \tag{37}$$

where $T^* = (T-T_\infty)/(T_0-T_\infty)$, $w^* = m-m_\infty$, and time t has been scaled with R^2/α_∞.

3.2. *Liquid phase*

The dimensionless energy equation is (omitting asterisks)

$$\frac{\partial^2 T_\ell}{\partial r^2}+\frac{2}{r}\frac{\partial T_\ell}{\partial r}+\frac{1}{r^2}\frac{\partial}{\partial \bar{\mu}}(1-\bar{\mu}^2)\frac{\partial T_\ell}{\partial \bar{\mu}} = Pe_\ell\left(u_{\ell r}\frac{\partial T_\ell}{\partial r}+u_{\ell\theta}\frac{1}{r}\frac{\partial T_\ell}{\partial \theta}\right)+\frac{\partial T_\ell}{\partial t}, \tag{38}$$

where $T_\ell^* = (T_\ell-T_\infty)/(T_0-T_\infty)$, $Pe_\ell = Re_\ell Pr_\ell$, $Re_\ell = U_\infty R/\nu_\ell$, $Pr_\ell = \nu_\ell/\alpha_\ell$, and time t has been scaled with R^2/α_ℓ. The above heat/mass-transfer equations are subject to the following boundary conditions, initial conditions and interface conditions.

3.3. *Boundary conditions, initial conditions and interface conditions*

For the vapour–gas phase

$$T = w = 0 \quad \text{as} \quad \xi \to \infty, \tag{39}$$

$$\frac{\partial T}{\partial \theta} = \frac{\partial w}{\partial \theta} = 0 \quad (\theta = 0, \pi), \tag{40}$$

$$T = w = 0 \quad (t = 0). \tag{41}$$

For the liquid phase

$$T_\ell < \infty \quad (r = 0; \quad \text{all } \theta), \tag{42}$$

$$\frac{\partial T_\ell}{\partial \theta} = 0 \quad (\theta = 0, \pi; \quad \text{all } r), \tag{43}$$

$$T_\ell = 1 \quad (t = 0). \tag{44}$$

The interface conditions, at $r = 1$, are

$$u_r = \frac{1}{m_i Sc}\frac{\partial w}{\partial r}, \tag{45}$$

$$\frac{\partial T_\ell}{\partial r} = -\frac{\phi_k Pr}{Ja}u_r+\phi_k\frac{\partial T}{\partial r}, \tag{46}$$

$$T = T_\ell = T_i. \tag{47}$$

In (46) $\phi_k = k_\infty/k_\ell$ and $Ja = C_p\Delta T/\lambda$. $\Delta T = T_0-T_\infty$.

3.4. *Expansion procedure for heat/mass-transfer analysis*

Let

$$T = \bar{T}_0(\xi, t) + \epsilon \sum_{n=0}^{\infty} T_n(\xi, t) P_n(\bar{\mu}), \tag{48}$$

$$w = \bar{w}_0(\xi, t) + \epsilon \sum_{n=0}^{\infty} w_n(\xi, t) P_n(\bar{\mu}), \tag{49}$$

$$T_\ell = \sum_{n=0}^{\infty} T_{ln}(\xi, t) P_n(\bar{\mu}). \tag{50}$$

On substituting (48)–(49) into (36) and (37), and using appropriate velocity fields, we obtain for the continuous phase

$$e^{2\xi} \frac{\partial \bar{T}_0}{\partial t} + Pr\, e^{-\xi} A_{00} \frac{\partial \bar{T}_0}{\partial \xi} = \frac{\partial^2 \bar{T}_0}{\partial \xi^2} + \frac{\partial \bar{T}_0}{\partial \xi}, \tag{51}$$

$$e^{2\xi} \frac{\partial T_n}{\partial t} + Pr\left(e^{-\xi} A_{00} \frac{\partial T_n}{\partial \xi} - e^{-\frac{1}{2}\xi} f_n \frac{\partial \bar{T}_0}{\partial \xi}\right) = T_n'' + T_n' - n(n+1) T_n \quad (n = 0, 1, 2, \ldots), \tag{52}$$

$$e^{2\xi} \frac{\partial \bar{w}_0}{\partial t} + Sc\, e^{-\xi} A_{00} \frac{\partial \bar{w}_0}{\partial \xi} = \frac{\partial^2 \bar{w}_0}{\partial \xi^2} + \frac{\partial \bar{w}_0}{\partial \xi}, \tag{53}$$

$$e^{2\xi} \frac{\partial w_n}{\partial t} + Sc\left(e^{-\xi} A_{00} \frac{\partial w_n}{\partial \xi} - e^{-\frac{1}{2}\xi} f_n \frac{\partial \bar{w}_0}{\partial \xi}\right) = w_n'' + w_n' - n(n+1) w_n \quad (n = 0, 1, 2, \ldots), \tag{54}$$

where the prime denotes differentiation with respect to ξ. For the drop interior we substitute (50) and velocity fields derived from (21) into (38). Then we multiply the resulting equation by $P_m(\bar{\mu})$ and integrate it, involving orthogonality of Legendre polynomials where appropriate, to generate the following set of equations:

$$\frac{\partial T_{\ell n}}{\partial t} - \frac{Pe_\ell (2n+1)}{r^2} \left\{ \sum_{I=0}^{\infty} \sum_{J=0}^{\infty} \left[\begin{pmatrix} n & I & J \\ 0 & 0 & 0 \end{pmatrix}^2 F_J T_{\ell I}' + \left(\frac{I(I+1)}{J(J+1)}\right)^{\frac{1}{2}} \begin{pmatrix} n & I & J \\ 0 & 1 & -1 \end{pmatrix} \begin{pmatrix} n & I & J \\ 0 & 0 & 0 \end{pmatrix} F_J' T_{\ell I} \right] \right\}$$
$$= T_{\ell n}'' + \frac{2}{r} T_{\ell n}' - n(n+1) T_{\ell n} \quad (n = 0, 1, 2, \ldots), \tag{55}$$

where

$$\begin{pmatrix} n_1 & n_2 & n_3 \\ m_1 & m_2 & m_3 \end{pmatrix}$$

are the 3-j symbols (Rotenberg *et al.* 1959; Talman 1968). The boundary conditions, initial conditions and interface conditions are as follows.

For the vapour–gas phase

$$\bar{T}_0 = T_n = 0, \quad \bar{w}_0 = w_n = 0 \quad \text{as} \quad \xi \to 0, \tag{56}$$

$$\bar{T}_0 = T_n = 0, \quad \bar{w}_0 = w_n = 0 \quad (t = 0). \tag{57}$$

The symmetry conditions $\partial T/\partial\theta = \partial w/\partial\theta = 0$ at $\theta = 0$ and π are satisfied by (48) and (49).

For the liquid phase

$$\frac{\partial T_{\ell 0}}{\partial r} = 0, \quad T_{\ell n} = 0, \quad n \geqslant 1 \quad (r = 0; \quad \text{all } \theta), \tag{58}$$

$$T_{\ell n} = \delta_{n0} \quad (t = 0). \tag{59}$$

Also, (43) is satisfied by (50).

The interface conditions, at $r = 1$, are the following: on substituting (49) and (50) into (45) and (47), and using appropriate flow fields, we obtain

$$\frac{\partial \bar{w}_0}{\partial \xi} = Sc\, A_{00}(\bar{w}_0 + m_\infty)\, \mathrm{e}^{\xi}, \tag{60}$$

$$\frac{\partial w_n}{\partial \xi} = Sc\,[A_{00}\, w_n - (\bar{w}_0 + m_\infty) f_n(0)]\, \mathrm{e}^{\xi} \quad (n = 0, 1, 2, \ldots), \tag{61}$$

$$\frac{\partial T_{\ell 0}}{\partial r} = \phi_k \left[-\frac{Pr}{Ja} A'_{00} + \left(\frac{\partial \bar{T}_0}{\partial \xi} + \epsilon \frac{\partial T_0}{\partial \xi} \right) \mathrm{e}^{-\xi} \right], \tag{62}$$

$$\frac{\partial T_{\ell n}}{\partial r} = \phi_k \epsilon \left[-\frac{Pr}{Ja} f_n(0) + \frac{\partial T_{\ell n}}{\partial \xi} \mathrm{e}^{-\xi} \right] \quad (n = 1, 2, 3, \ldots), \tag{63}$$

$$\bar{T}_0(0, t) + \epsilon \sum_{n=0}^{\infty} T_n P_n(\bar{\mu}) = \sum_{n=0}^{\infty} T_{\ell n} P_n(\bar{\mu}). \tag{64}$$

Equations (51)–(55) are subject to the conditions (56)–(64).

4. Evaluation of $U_\infty(t)$

As discussed in Part 1, the velocity of the drop at any instant is a function of the radial flow field induced by condensation. This velocity, relative to the quiescent ambient mixture of steam and air, is governed by the following equation of motion:

$$\frac{\mathrm{d}U_\infty(t)}{\mathrm{d}t} = \left(1 - \frac{\rho_\infty}{\rho_\ell}\right) g - \frac{3}{8} \frac{\rho_\infty}{\rho_\ell} C_{\mathrm{D}} \frac{U_\infty^2(t)}{R}, \tag{65}$$

where the added-mass force, pressure-gradient force and the Basset history force (Basset 1888, see also Clift, Grace & Weber 1978) have all been neglected. The neglect is based on the large difference in density between that of the drop and of the gas–vapour mixture. The drag coefficient C_{D} is defined by

$$C_{\mathrm{D}} = \frac{\text{drag force}}{\frac{1}{2}\rho_\infty U_\infty^2(t)\, \pi R^2}. \tag{66}$$

From Milne-Thomson (1968), after suitable rearrangement,

$$C_{\mathrm{D}} = \frac{-4\mathrm{e}^{2\xi}}{Re_\infty^2} \left[\int_0^\pi p(\xi, \theta) \cos\theta \sin\theta \, \mathrm{d}\theta + \int_0^\pi (u_r u_r \cos\theta - u_r u_\theta \sin\theta) \sin\theta \, \mathrm{d}\theta \right.$$
$$\left. - \int_0^\pi \left(2 \frac{\partial u_r}{\partial r} \cos\theta - \left(r \frac{\partial}{\partial r} \left(\frac{u_\theta}{r} \right) + \frac{1}{r} \frac{\partial u_r}{\partial \theta} \right) \sin\theta \right) \sin\theta \, \mathrm{d}\theta \right], \tag{67}$$

where p is dimensionless pressure. We calculate C_{D} also by the series-truncation

method. For this calculation C_D is transformed in terms of f_n and g_n, and at the interface, $\xi = 0$, C_D becomes

$$C_D = \frac{8}{3Re_\infty}\left\{[g_1(0)+g_1'(0)+\tfrac{1}{2}A_{00}(\tfrac{1}{4}f_1(0)-f_1''(0))]+\left[A_{00}(\tfrac{3}{2}f_1(0)-f_1'(0))\right.\right.$$
$$\left.\left.-\tfrac{3}{2}Re_\infty\left(\sum_{n=1}^{\infty} f_n(0)\frac{1}{n+\frac{1}{2}}\left(\frac{f_{n+1}'(0)}{2n+3}-\frac{f_{n-1}'(0)}{2n+1}\right)\right)\right]-(2g_1(0)+3f_1(0))\right\}. \quad (68)$$

The initial condition for the equation (65) is

$$U_\infty(0) = \frac{2}{3}\frac{\rho_\ell-\rho_\infty}{\mu_\infty}\frac{\mu_\ell+\mu_\infty}{2\mu_\infty+3\mu_\ell}gR^2. \quad (69)$$

The Runge–Kutta method was employed for the solution of (65).

5. A brief discussion of numerical procedures

Equations (24)–(27) subject to conditions (28)–(35) for the flow fields, and (51)–(55) subject to conditions (56)–(64) for the heat/mass transfer are solved simultaneously through finite-difference numerical procedures. A simultaneous solution, at each time step, is needed in view of the coupling of the variables at the interface. In the actual solution a truncation of order n_0 is defined by setting all f_n, F_n, g_n, G_n, T_n, w_n, and $T_{\ell n}$ equal to zero for $n > n_0$. The order n_0 depends on ϵ, Pe, Pe_ℓ and on the strength of condensation fluxes Re_c. The value of n_0 is determined by letting it increase until there is no appreciable change in the calculated results. In this study $n_0 = 6$ was found to be adequate for describing high rates of condensation ($Re_c \sim 5$), while $n_0 = 4$ was sufficient for the complete Stokes-regime problem. The governing equations (24)–(27) and (51)–(55), in their truncated form, present a set of nonlinear coupled differential equations. The finite-difference method employs the three-point central-difference scheme for the spatial derivatives and the backward-difference for the temporal derivatives. The strongly implicit procedure proposed by Stone (1968) was adopted for the solutions of the finite-difference equations. The resultant tridiagonal matrix for each mode is solved from $n = 0$ to $n = n_0$, one mode at a time, while holding the values of all other modes constant until all the boundary conditions appropriate for the given mode are satisfied. The same operation is performed on the next mode, with a relaxation of the calculated values for the previous mode. During the above primary iteration, the nonlinear terms are held constant. At the end of each primary iteration cycle the nonlinear terms are relaxed and the primary iteration cycle is then repeated until the desired convergence criterion is met. The $\xi \to \infty$ condition, in this study, was set finally at $\xi = 5.5$ after some numerical experimentation.

Since the governing equations are all in a single-dimension (r-direction) form, the droplet interior is divided into $L-1$ equal radial spacings and the continuous phase into $M-L$ equal spacings in ξ (see figure 1 for details). The iteration procedure for each time step involves the flow-field calculation, for both phases, at the beginning of each iteration cycle. The flow equations (24)–(27) with boundary conditions (28)–(35) can be solved explicitly once A_{00} and $f_n(0)$ are known. The values of these quantities are guessed for the first iteration of the first time step. For subsequent iterations the values of the previous iteration are used. The temperature and the species equations are then solved for each grid point by using the most recent flow solutions.

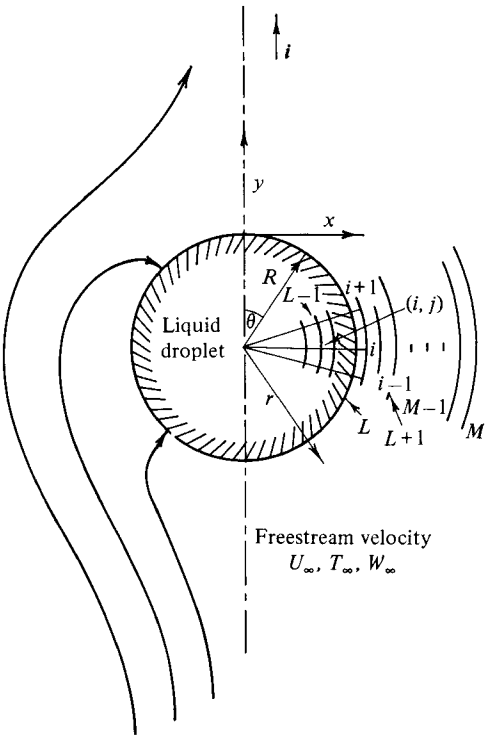

FIGURE 1. Geometry and numerical grid description.

At the interface the two compatibility conditions (60) and (62) must be satisfied. In a fully transient treatment repeated iteration is required to enforce a strict conservation of mass and energy across the interface. A strong-coupling scheme for condensation velocities A_{00} and $f_n(0)$, mass fraction of air $m_i(T_i, p_\infty)$ and interface temperature T_i must be implemented. The heat-flux continuity equation (62) must be recognized as only a surface condition. Therefore, in order to satisfy conservation-of-energy requirements strictly, the energy equation must be written as appropriate to a control volume. The control volume chosen here is enclosed by two concentric spherical surfaces. The outer surface of this shell coincides with the drop surface, while the locus of the inner is the bisection of the grid line connecting the outer surface to the first inner grid point, as shown in the shaded area of figure 1. Equations (62) and (63) are the outer-surface boundary conditions for this volume. The interface condensation-velocity terms A_{00} and $f_n(0)$ are then expressed in terms of the following set of special iteration equations to ensure efficient and fast convergence. Equations (6) and (61) are rewritten as

$$A_{00} = \frac{A^0_{00}}{\bar{w}^0_0 + m_\infty}(\bar{w}^0_0 - \bar{w}_0) + \frac{1}{Sc\,(\bar{w}^0_0 + m_\infty)}\frac{\partial \bar{w}_0}{\partial \xi}\mathrm{e}^{-\xi}, \tag{70}$$

$$f_n(0) = \frac{f^0_n(0)}{w^0_n}(w^0_n - w_n) - \frac{1}{Sc\,(\bar{w}^0_0 + m_\infty)}\frac{\partial w_n}{\partial \xi}\mathrm{e}^{-\xi} + \frac{A^0_{00}\,w_n}{\bar{w}^0_0 + m_\infty}, \tag{71}$$

where superscript 0 represents the previous iterate value.

The iteration procedure for the mass fraction and the surface temperature employs

the Clausius–Clapeyron equation and the approximation that the gas–vapour mixture behaves like an ideal gas as follows:

$$\bar{T}_0 = \frac{T^*_\infty A'_2}{[A'_2 - T^*_\infty \ln((1-\bar{w}'_0)/(1+A_2\bar{w}'_0)A'_1)]\Delta T} - \frac{T^*_\infty}{\Delta T}, \tag{72}$$

$$T_n = \frac{-w_n(1+A_2)(\bar{T}^*_0)^2}{(1+A_2\bar{w}'_0)(1-\bar{w}'_0)A'_2\Delta T}, \tag{73}$$

where T^*_∞ is the absolute temperature in the bulk, $A'_1 = p_{v,\infty}/p_\infty$, $A'_2 = \lambda/\bar{R}$, $A_2 = M_v/M_g - 1$, $\bar{w}'_0 = \bar{w}_0 + m_\infty$, $\bar{T}^*_0 = \bar{T}_0\Delta T + T^*_\infty$; $\Delta T = T_0 - T_\infty$, λ is the latent heat of vaporization, $\bar{R}$ is the gas constant, M_v and M_g are the molecular weights of vapour and gas respectively, and $p_{v,\infty}$ is the vapour pressure of steam in the bulk. The iteration equations themselves are generated by linearizing the equations of mass fraction of the non-condensable gas at the interface about the previous iterations. These are

$$\begin{aligned}\bar{w}_0 &= \bar{w}^0_0 + \frac{A'_2\Delta T}{(\bar{T}^*_0)^2}\left(\bar{w}^0_0 + m_\infty - \frac{1+A_2(\bar{w}^0_0+m_\infty)}{1+A_2}\right)[1+A_2(\bar{w}^0_0+m_\infty)](\bar{T}_0 - \bar{T}^0_0)\\ &= g_1\bar{T}_0 + g_2, \quad g_2 = -g_1\bar{T}^0_0 + \bar{w}^0_0,\end{aligned} \tag{74}$$

$$\begin{aligned}w_n &= w^0_n + \frac{[1+A_2(\bar{w}^0_0+m_\infty)](1-\bar{w}^0_0-m_\infty)A'_2\Delta T}{(1+A_2)(\bar{T}^*_2)^2}(T_n - T^0_n)\\ &= g_{1n}T_n + g_{2n}, \quad g_{2n} = -g_{1n}T^0_n + w^0_n,\end{aligned} \tag{75}$$

$$g_1 = \frac{A'_2}{(\bar{T}^*_2)^2}\left(\bar{w}^0_0 + m_\infty - \frac{1+A_2(\bar{w}^0_0+m_\infty)}{1+A_2}\right)[1+A_2(\bar{w}^0_0+m_\infty)], \tag{76}$$

$$g_{1n} = \frac{[1+A_2(\bar{w}^0_0+m_\infty)][1-\bar{w}^0_0-m_\infty]A'_2\Delta T}{(1+A_2)(\bar{T}^*_0)^2}.$$

Equations (51–54) can be written as the following finite-difference equations:

$$T^{n+1}_i = a_{1i}T^{n+1}_{i+1} + a_{2i}T^{n+1}_{i-1} + a_{3i} \quad (i = 1, 2, \ldots, M; \quad i \neq L), \tag{76}$$

$$w^{n+1} = b_{1i}w^{n+1}_{i+1} + b_{2i}w^{n+1}_{i-1} + b_{3i} \quad (i = L+1, \ldots, M), \tag{77}$$

where $\bar{T}$ stands for $\bar{T}_0$ or T_n and w for $\bar{w}_0$ or w_n respectively.

The time-dependent control-volume energy-balance equations with surface boundary conditions (62) and (63), the auxiliary equations (70)–(75) and the equations (76) and (77) can be written in finite-difference forms. After rearrangement, we obtain the following equations for the interface temperature:

$$T^{n+1}_L = A_L T^{n+1}_{L+1} + B_L T^{n+1}_{L-1} + E_L w^{n+1}_{L+1} + F_L w^{n+1}_L + G_L, \tag{78}$$

$$w^{n+1}_L = g_1 T^{n+1}_L + g_2. \tag{79}$$

Here g_1 and g_2 should be replaced by g_{1n} and g_{2n} respectively, whenever w stands for w_n. The superscript and subscript represent the time-step number and the node point respectively. With temperatures and mass fractions of non-condensable gas known for each node point, the condensation velocities A_{00} and $f_n(0)$ are updated using (70) and (71). The iteration procedure is continued until $|1 - A_{00}/A^0_{00}|$ and $|1 - f_n(0)/f^0_n(0)|$ are less than 10^{-3}.

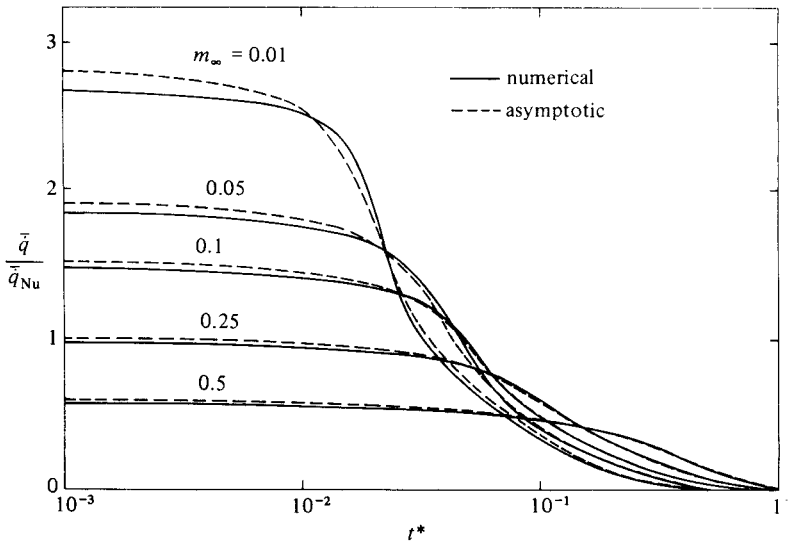

FIGURE 2. Dimensionless heat transfer *vs.* dimensionless time: numerical and asymptotic results; $Re_{nc} = 0.5$, $T_0 = 30$ °C, $T_\infty = 100$ °C.

6. Results and discussion

Here we shall discuss numerical comparisons and temperature fields. The discussion about the physical insights gained from a study of condensation on a moving droplet has already been presented in Part 1. The initial and ambient thermodynamic conditions are kept the same as in Part 1. This enables a direct comparison of numerical results with those of the asymptotic analysis.

For the numerical calculations, the average heat transfer $\bar{q}$ is computed from

$$\bar{q} = \frac{-\mu_\infty \lambda A_{00}}{R} + \frac{k\Delta T}{R}\left[\frac{\partial \bar{T}_0}{\partial \xi} + \epsilon \frac{\partial T_0}{\partial \xi}\right]_{\xi=0}, \tag{80}$$

while $\bar{q}_{Nu}$ remains the same as before.

Figures 2 and 3 show the comparisons between the numerical and asymptotic results for dimensionless heat transfer as a function of dimensionless time. The time-independent Reynolds number Re_{nc}, based on the steady terminal velocity $U_{\infty 0}$ is 0.5 for figure 2 and 0.1 for figure 3. The agreement between the results is very good, particularly for the low rates of condensation (low Re_c, high m_∞). The presence of a large non-condensable mass fraction in the bulk causes the radial-flow field to be weakened. In turn, the internal circulation inside the drop is weaker, and the corresponding liquid-side Péclet number Pe_ℓ is smaller. The asymptotic solution should be capable of representing this situation very well, and it is seen to do so. Any discrepancy that is observed between the numerical and asymptotic results could be explained in the following manner. First recall the differences in methodology between the two techniques as implemented in our study. For the singular perturbation solutions, the flow fields in both the phases and the heat/mass transport in the continuous phase were all assumed quasi-steady. Only the liquid-phase heat transfer was treated as transient there. The velocities and temperatures were expanded in terms of the instantaneous Reynolds number $Re_\infty(t)$, and the terms smaller than $O(Re_\infty(t))$ were neglected. The numerical solution, on the other hand, treats both the

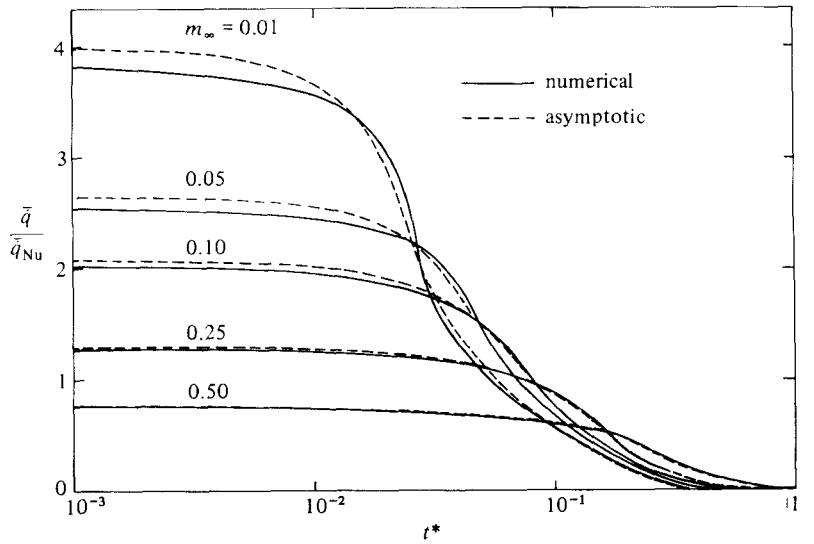

FIGURE 3. Dimensionless heat transfer *vs.* dimensionless time; numerical and asymptotic results; $Re_{nc} = 0.1$, $T_0 = 30$ °C, $T_\infty = 100$ °C.

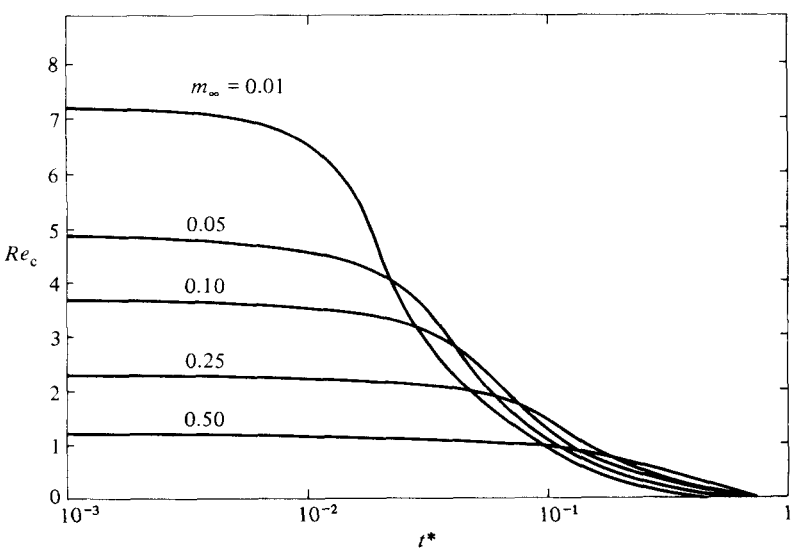

FIGURE 4. Variation of *condensation-induced* Reynolds number Re_c with dimensionless time for time-independent Reynolds number $Re_{nc} = 0.5$, $T_0 = 30$ °C, $T_\infty = 100$ °C.

phases as fully transient for flow and heat/mass transport. The technique relies on the series-truncation method in which the series expansion has been truncated only after the sixth term. On these bases, the deviations between the calculated results may be attributed to two possible causes: (*a*) presence of a strong condensation field leading to a high Re_c (~ 5) and the inability of the asymptotic solution to accommodate such high Re_c values; (*b*) invoking the quasi-steady assumption for the continuous phase. The quasi-steady assumption may become invalid at very high condensation rates. Yet another observation that can be made from figures 2 and 3 is that the

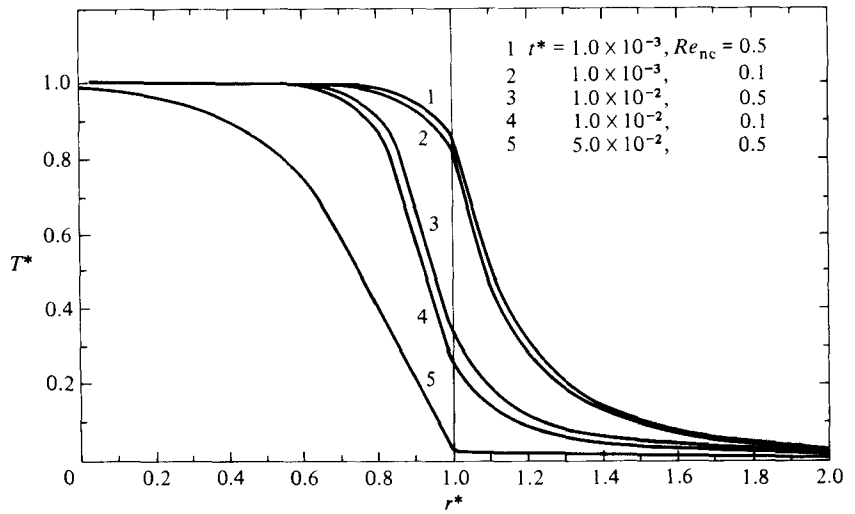

FIGURE 5. Dimensionless temperature T^* *vs.* radial distance r^* from drop centre; $T_0 = 30\ °C$, $T_\infty = 100\ °C$, $m_\infty = 0.01$.

asymptotic results overpredict the heat transfer for very short times ($t^* < 10^{-2}$) as compared with the numerically calculated values. However, higher heat transfer leads to a rapid increase of surface temperature and a consequent decrease in the thermal driving force. With increasing t^* the asymptotic results therefore underpredict. But again, at a much higher t^*, the numerically calculated values are less for this same reason. This explains the 'wraparound' effect noted in figures 2 and 3.

Figure 4 shows the variation of the condensation-induced Reynolds number Re_c with dimensionless time t^* for Re_{nc} equal to 0.5 and m_∞ varying from 0.01 to 0.5. Lower non-condensable mass fractions lead to higher Re_c. As the drop equilibrates with the ambient environment and condensation ceases, the Re_c value becomes zero. The drop continues to translate at its terminal velocity Re_{nc} beyond this point.

Figure 5 shows the variation of the numerically computed dimensionless temperature with radial distance from the drop centre. The results presented are for the drop equatorial plane ($\theta = 90°$). The interface is given by $r^* = 1$. A decrease in the non-dimensional temperature corresponds to an increase in actual temperature. Conduction heat transfer is seen to be the dominant mechanism for the droplet interior. This is as would be expected. The steep temperature gradient in the vapour–gas phase is due to the condensation-induced radial velocity that convects the heat to the droplet surface.

The computation time typically ranges within 1–2 minutes on an AMDHAL machine for calculating one complete characteristic. The time required for convergent solutions increases with increasing Re_c and with decreasing m_∞ (relatively vigorous condensation).

Sponsorship of this work by the National Science Foundation under Grants ENG77-23137 and MEA 8023861 is gratefully acknowledged.

REFERENCES

BASSET, A. B. 1888 *A Treatise on Hydrodynamics*, vol. 2, chap. 22. Deighton Bell. [Republished 1961 by Dover.]

CHUNG, J. N., AYYASWAMY, P. S. & SADHAL, S. S. 1984 Laminar condensation on a moving drop. Part 1. Singular perturbation technique. *J. Fluid Mech.* **139**, 105–130.

CLIFT, R., GRACE, J. R. & WEBER, M. E. 1978 *Bubbles, Drops and Particles*, p. 287. Academic.

DENNIS, S. C. R., WALKER, J. D. A. & HUDSON, J. D. 1973 Heat transfer from a sphere at low Reynolds numbers. *J. Fluid Mech.* **60**, 273–283.

MILNE-THOMSON, L. M. 1968 *Theoretical Hydrodynamics*. Macmillan.

ROTENBERG, M., BIVINS, R., METROPOLIS, N. & WOOTEN, J. K. 1959 *The 3-j and 6-j symbols*. MIT Press.

SADHAL, S. S. & AYYASWAMY, P. S. 1983 Flow past a liquid drop with a large non-uniform radial velocity. *J. Fluid Mech.* **133**, 65–81.

STONE, H. L. 1968 Iterative solution of the implicit approximation of multidimensional partial differential equations. *Siam J. Numer. Anal.* **5**, 530–558.

TALMAN, J. D. 1968 *Special Functions*. Benjamin.

VAN DYKE, M. 1965 A method of series-truncation applied to some problems in fluid mechanics. *Stanford Univ. Rep.* SUDAER no. 247.